

Quantum criticality with a twist - interplay of correlations and Kohn anomalies in three dimensions

T. Schäfer^a, A. A. Katanin^b, K. Held^a, and A. Toschi^a

^a*Institute of Solid State Physics, TU Wien, 1040 Vienna, Austria and*

^b*Institute of Metal Physics, 620990, Kovalevskaya str. 18, Ekaterinburg, Russia
Ural Federal University, 620002, Mira str. 19, Ekaterinburg, Russia*

(Dated: August 7, 2018)

A general understanding of quantum phase transitions in strongly correlated materials is still lacking. By exploiting a cutting-edge quantum many-body approach, the dynamical vertex approximation, we make an important progress, determining the quantum critical properties of the antiferromagnetic transition in the fundamental model for correlated electrons, the Hubbard model in three dimensions. In particular, we demonstrate that -in contradiction to the conventional Hertz-Millis-Moriya theory- its quantum critical behavior is driven by the Kohn anomalies of the Fermi surface, even when electronic correlations become strong.

PACS numbers: 71.27.+a, 71.10.Fd, 73.43.Nq

Introduction. The underlying quantum mechanical nature of the physical world is often elusive at the macroscopic scale of every-day-life phenomena. In the case of solid state physics, the most striking manifestations of its quantum origin are confined to very low temperatures, where thermal fluctuations are frozen. An important exception is realized where thermodynamic phase transitions (e.g. to a magnetic state) are driven to occur at zero temperature, at a quantum critical point (QCP)[1–4]: The corresponding quantum critical fluctuations become then abruptly visible also at sufficiently high temperatures, representing one of the most exciting subjects in condensed matter physics.

While QCPs are actually found experimentally in the phase-diagrams of several compounds[1], a general theoretical treatment of their physics is still lacking. Consequently, the analysis of experiments often remains based on a mere fitting of the exponents controlling the critical behavior at the QCPs, preventing a general comprehension of the phenomenon. The major challenge, in this respect, is the competition of several equally important physical mechanisms, because, at the QCP, both long-ranged space- and time-fluctuations must be treated on an equal footing. In fact, this is only possible in limiting cases, such as in the perturbative regime, by means of Moriya[5]-Dzyaloshinskii-Kondratenko[6] theory and the famous renormalization group (RG) treatment by Hertz[7] and Millis[8]. However, an actual comprehension of the experiments based only on these theories is highly problematic, for two reasons. First of all, most quantum critical materials are strongly correlated. This is certainly the case for the (antiferro)magnetic quantum critical points (QCPs) of transition metals under pressure, such as $\text{Cr}_{1-x}\text{V}_x$ [9–12] and heavy fermion compounds under pressure or in a magnetic field, such as in $\text{CeCu}_{6-x}\text{Au}_x$ [13] and YbRh_2Si_2 [14, 15]. It has been established that one effect of strong correlations, namely the breakdown of the “large” Fermi-surface containing

both conduction and f -electrons and the associated local quantum criticality [16, 17], may lead to different critical exponents. Nonetheless, we are still far away from identifying the universality classes beyond the conventional Hertz-Millis-Moriya (HMM) theory.

Besides electronic correlations, the physics of QCPs can also be affected by specific properties of their Fermi surfaces (FS), such as van Hove singularities, nesting, or Kohn points. The effects thereof are often of minor importance at high- T , but can be amplified in the low- T regime. While van Hove singularities and nesting require special forms of the electronic spectrum, Kohn points are more generic and easily occur in three-dimensional ($3d$) [18, 19] and two-dimensional ($2d$) systems [20–22]. Kohn points are defined as the points of the FS that (i) are connected by the spin-density wave (SDW) vector \mathbf{Q} and (ii) beyond that have *opposite* Fermi velocities. These points are associated to the textbook “Kohn anomalies” of the susceptibilities [18, 23], also called $Q = 2k_F$ anomalies, which is the momentum where they occur for an isotropic FS. The effect of Kohn anomalies on the phonon dispersion is well known [18] and the breakdown of standard HMM theory has been conjectured [1, 8].

In this paper we make significant progress towards a better understanding of QCPs. We demonstrate that FS features in $3d$ lead to an unexpected universality class of its magnetic QCP, which also holds in the non-perturbative regime. In principle, the complexity of the competing microscopic mechanisms underlying a quantum phase transition of correlated electrons calls for a quantum many-body technique capable of treating *both*, extended spatial and temporal fluctuations, *beyond* the weak-coupling, perturbative regime. The approach we exploit here is the dynamical vertex approximation (DVA) [25–29], which is a diagrammatic extension [25, 30–39] of dynamical mean field theory (DMFT) [40, 41] built on its two-particle vertices [42, 43]. It has been already successfully used to study classical, finite temperature criticality of strongly

correlated systems in $3d$ [44–46], as well as long-range antiferromagnetic (AF) fluctuations and their effect on the electronic self-energy in $2d$ [26, 47]. In fact, DGA builds up non-local corrections at all length scales on top of DMFT [42], which in turn captures, in a non-perturbative fashion, all purely local temporal correlations [41]. Hence, per construction, the scheme is particularly suited to the study of quantum critical phenomena.

The obtained phase diagram as a function of doping displays a progressive suppression of the Néel temperature (T_N), a crossover to an incommensurate SDW-order, and eventually the vanishing of the magnetic order at a QCP with $\sim 20\%$ doping. Upon doping, the critical scaling properties of the second-order magnetic transition change abruptly from the ones expected for the universality class of the $3d$ Heisenberg model, a “classical” finite- T phase transition, to a quantum critical behavior visible in a relatively broad funnel-shaped temperature region above the QCP. Our results unveil the importance of Kohn anomalies for the scaling properties of the QCP. In particular, the T -dependence of the magnetic susceptibility ($\chi_{\mathbf{Q}} \propto T^{-\gamma}$) at the SDW wave-vector \mathbf{Q} and of the correlation length ($\xi \propto T^{-\nu}$) largely deviate from the typical behavior expected from the HMM theory for AF quantum phase transitions in $3d$.

Phase diagram. We focus here on the magnetic transitions in the Hubbard model on a simple cubic lattice:

$$H = -t \sum_{\langle ij \rangle > \sigma} c_{i\sigma}^\dagger c_{j\sigma} + U \sum_i n_{i\uparrow} n_{i\downarrow}, \quad (1)$$

where t is the hopping amplitude between nearest neighbors, U the local Coulomb interaction, $c_{i\sigma}^\dagger$ ($c_{i\sigma}$) creates (annihilates) an electron with spin $\sigma = \uparrow, \downarrow$ at site i , and $n_{i\sigma} = c_{i\sigma}^\dagger c_{i\sigma}$; the average density is $n = \langle n_{i\uparrow} \rangle + \langle n_{i\downarrow} \rangle$. Hereafter all energies are measured in units of $D = 2\sqrt{6}t \equiv 1$, twice the standard deviation of the non-interacting density of states; we employ $U = 2.0$, for which the highest T_N at half-filling is found in both, DMFT and DGA [44]. We do not consider phase-separation[48], charge-ordering[49, 50] or disorder[51]-induced effects.

To explore the magnetic phase diagram, we employ DMFT with exact diagonalization (ED) as impurity solver and DGA in its ladder-approximation version supplemented by Moriyaesque λ -corrections, see Refs. [26, 28, 52] for the implementation used here as well [see Supplemental Material, Sec. II (ii) for more specific details [53]]. This approach includes spin-fluctuations and was successfully applied to calculate the critical exponents in $3d$ before [44]. Superconducting fluctuations are treated at the DMFT level (the full parquet DGA [57, 58] which would incorporate these fluctuations is numerically too demanding for the required momentum-grids at the QCP).

The primary quantity we calculate is the static, fully momentum-dependent magnetic susceptibility $\chi_{\mathbf{q}} \equiv$

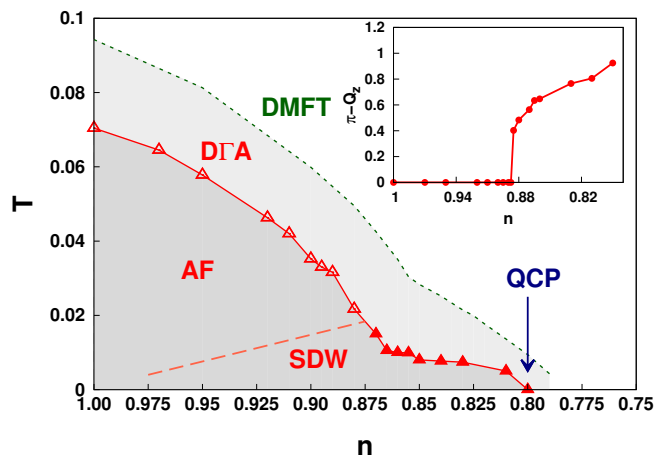


FIG. 1. (Color online) Phase diagram of the $3d$ Hubbard model at $U = 2D$, showing the leading magnetic instability as a function of the density n in both DMFT and DGA. Inset: Evolution of the magnetic ordering vector along the instability line of DGA, showing a transition from a commensurate AF with $Q_z = \pi$ (open triangles in the main panel) to incommensurate SDW with $Q_z < \pi$ (full triangles in the main panel). The dashed red line indicates the presumptive crossover between AF and SDW.

$\chi_{\mathbf{q}}(\omega=0)$, as a function of temperature T . It has a maximum at a specific (temperature-dependent) wave-vector $\mathbf{q} = \mathbf{Q}_T$, and diverges at $T = T_N$, marking the occurrence of a second-order phase-transition towards magnetism with ordering vector \mathbf{Q}_{T_N} .

Figure 1 shows the corresponding divergence points in the T - n phase-diagram both for DMFT (green) and DGA (red). By progressively reducing n , T_N decreases and two regions of the magnetic ordering can be distinguished: (i) close to half-filling, we observe an instability at $\mathbf{Q}_{T_N} = (\pi, \pi, \pi)$ i.e., to commensurate AF (open triangles); (ii) at higher doping ($n \lesssim 0.88$) the ordering vector is shifted to $\mathbf{Q}_{T_N} = (\pi, \pi, Q_z < \pi)$, i.e. an incommensurate SDW (filled triangles). The inset of Fig. 1 quantifies the incommensurability $\pi - Q_z$, i.e., the deviation from a checkerboard AF order.

Eventually, ordering is suppressed completely as $T_N \rightarrow 0$, leading to the emergence of a QCP at $n_c^{\text{DGA}} \approx 0.805$. We note that the critical filling in DMFT is comparable to that obtained before [59] for a similar interaction strength ($U = 2.04D$).

Critical properties. Let us now turn to the (quantum) critical behavior. We select representative temperature cuts at four different dopings ($n = 1.0/0.87/0.805/0.79$) chosen on both the ordered and the disordered side of the QCP. Along these four paths we compute two fundamental observables, which yield the (quantum) critical exponents γ and ν of the magnetic transition: (i) the spin-susceptibility $\chi_{\mathbf{Q}_T} \propto (T - T_N)^{-\gamma}$ at its maximum, reached at the T -dependent wave-vector \mathbf{Q}_T , and (ii) the corresponding correlation length, $\xi \propto (T - T_N)^{-\nu}$. The

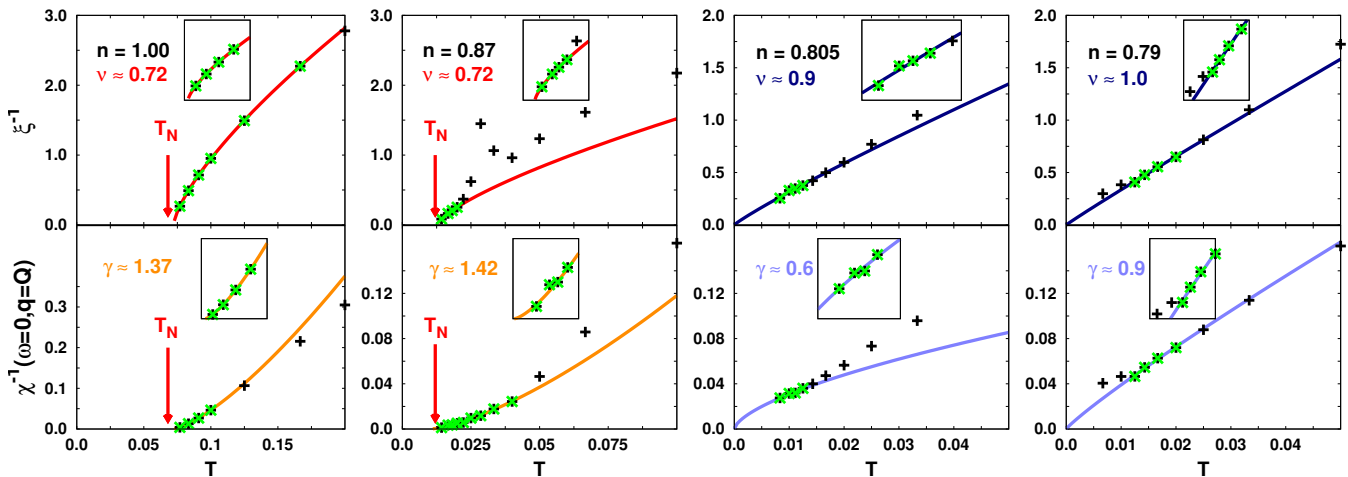


FIG. 2. (Color online) Inverse correlation length (ξ^{-1} , upper panels) and maximal susceptibility (χ^{-1} , lower panels) computed in DGA as a function of T for different n . The solid lines show the fits for extracting the critical exponents ν and γ (using the respective green points). The insets show zooms of the four respective lowest temperature points.

latter is calculated via $\chi_{\mathbf{Q}_T+\mathbf{q}} = A(\mathbf{q}^2 + \xi^{-2})^{-1}$.

Figure 2 shows the T -dependence of ξ^{-1} (upper panels) and $\chi_{\mathbf{Q}_T}^{-1}$ (lower panels). Note that, apart from its intrinsic T -dependence, the susceptibility is also affected by the T -dependence of the wave vector \mathbf{Q}_T , with the further complication that the dominating wave-vector changes with both n and T .

In the half-filled case (leftmost panels of Fig. 2) both ξ and $\chi_{\mathbf{Q}_T}$ display a critical behavior compatible with the 3d Heisenberg universality class when approaching the classical (finite- T) antiferromagnetic phase transition at $T_N(n=1) \approx 0.072$. The numerically extracted critical exponents of $\nu \approx 0.72$ and $\gamma \approx 1.37$ are consistent with previous calculations [44, 46], cf. our overview in Fig. 3 below.

Significant changes are observed at a doping, where the SDW-order appears ($n \simeq 0.87$, second column of Fig. 2). Here, by inspecting $\xi^{-1}(T)$ and $\chi^{-1}(T)$, a clear crossover is found between the high-temperature region ($T > 0.04$), where commensurate AF fluctuations dominate [maximum of $\chi_{\mathbf{q}}$ at (π, π, π)], to the low-temperature regime ($T < 0.025$) where incommensurate fluctuations at $(\pi, \pi, Q_z < \pi)$ outpace these before approaching the phase-transition. At the crossover, ξ^{-1} shows a maximum in Fig. 2, which is, however, not an indication of a decreasing correlation length, but rather reflects the inapplicability of our standard definition of ξ : In the vicinity of the AF-to-SDW crossover, we have a double-peak structure in $\chi_{\mathbf{q}}$ (not shown) at $Q_z = \pi$ and $Q_z \sim \pi - 0.4$ which altogether appears in the form of a large peak width, i.e., a large ξ^{-1} .

Despite the apparently more complex temperature-behavior of ξ and χ , and the onset of an incommensurate order, the critical exponents at low T are not altered at all ($\nu \approx 0.72, \gamma \approx 1.42$) with respect to the 3d Heisenberg

values. This is ascribed to the persistence of a classical phase-transition at $T_N(n=0.87) \approx 0.012$, which still belongs to the same universality class as the commensurate one. At higher T a linear behavior of the inverse susceptibility (which is characteristic for a mean-field theory for bosonic degrees of freedom) is eventually recovered.

Quantum criticality. Before turning to our DGA data at the QCP, let us briefly discuss the analytical results for the non-uniform susceptibility in the random phase approximation (RPA). We start by recalling that the standard HMM approach relies on the expansion [1, 5–8]

$$\chi_{\mathbf{Q}+\mathbf{q}}(\omega) = A(\mathbf{q}^2 + \xi^{-2} + i\omega/|\mathbf{q}|^{z-2})^{-1}, \quad (2)$$

where the first and third term in the denominator are determined by the band dispersion (under the assumption that no Kohn points exist). The T -dependence of the correlation length is $\xi^{-1} \propto T^\nu$ with $\nu = (d+z-2)/(2z) = 3/4$ ($d=3$ and $z=2$ for a SDW). It originates from the (para)magnon interaction, dominating over the T -dependence from the bare susceptibility. Since $d+z > 4$ we are above the upper critical dimension, and quantum criticality can be described by a bosonic mean-field theory.

As shown in the Supplemental Material [53], for the Kohn points on the FS spin fluctuations are, however, enhanced due to their antiparallel Fermi velocities, and their quantum critical behavior changes dramatically. Moreover, as our DGA calculations below demonstrate, the Kohn quantum critical behavior survives also in the strongly correlated regime. While the (possible) inapplicability of HMM in the presence of Kohn points has been pointed out before [1, 8], their implication on the quantum critical behavior in 3d and particularly the critical exponents have not been analyzed hitherto.

For the simple cubic lattice, which we consider here for

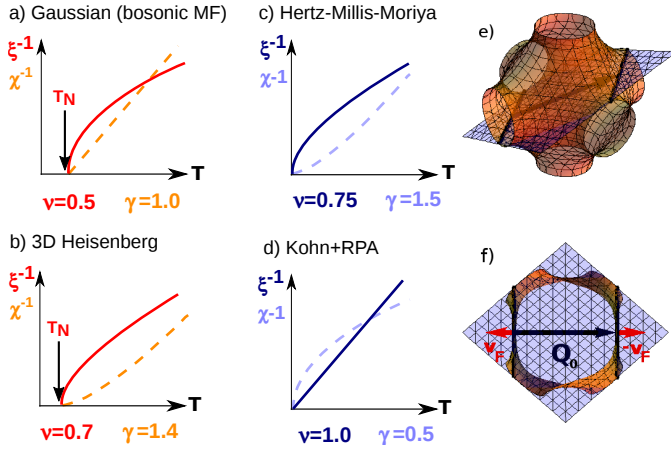


FIG. 3. (Color online) **(a, b)** Magnetic correlation length ξ and maximal magnetic susceptibility χ vs. T comparing the critical exponents ν and γ for a classical finite-temperature phase transition in (a) mean-field theory and (b) for the 3d Heisenberg model. **(c, d)** Quantum critical behavior comparing (c) standard HMM theory and (d) our scenario with Kohn line anomaly. **(e)** Visualization of (one out of four pairs of) Kohn lines in the 3d FS of the simple cubic lattice with nearest-neighbor hopping and the connecting SDW vector \mathbf{Q}_0 . **(f)** 2d cut with the Kohn-line of (e) and the corresponding (opposite) Fermi-velocities.

the numerical comparison with the DGA below, there are four pairs of lines of Kohn points ($\pm K_x, \mp K_x - \pi, -Q_z/2$) and ($\pi \pm K_x, \mp K_x, Q_z/2$) which are connected by the ground-state spin density wave-vectors $\mathbf{Q}_0 = (\pi, \pi, Q_z)$ (and symmetrically equivalent wave-vectors) and have opposite Fermi velocity, see Fig. 3 e) and f). The leading contributions in the momentum and T -dependence of χ^{-1} are non-trivial already in RPA. They stem from the vicinity of the lines' endpoints $(0, \pi, \pm Q_z/2)$ and $(\pi, 0, \pm Q_z/2)$, yielding (see Supplemental Material [53]):

$$\chi_{\mathbf{Q}_T+\mathbf{q}} \simeq \left[(\chi_{\mathbf{Q}_0}^{-1})_{T=0} + AT^{1/2} + BT^{-3/2}q_z^2 \right]^{-1}. \quad (3)$$

Here $\mathbf{Q}_T = \mathbf{Q}_0 + (0, 0, \delta Q_z)$, with $\delta Q_z = -2CT$ describing a shift of the wave-vector with the temperature and A, B, C are positive factors, containing weak, $\ln \ln(1/T)$, corrections. The susceptibility Eq. (3) is in stark contrast to the standard expansion Eq. (2). It is strongly anisotropic in momentum and strongly T -dependent due to non-analytic momentum- and temperature dependences of the bare susceptibility in the presence of Kohn anomalies. For $q_z = 0$ we obtain the critical exponent $\gamma = 1/2$ for the susceptibility, whereas the critical exponent for ξ (defined in the direction of the z axis) is $\nu = 1$. These exponents are strikingly different from those of HMM theory, $\nu = 3/4, \gamma = 2\nu = 3/2$. Even their relative magnitude is reversed, see Fig. 3 c) and d).

A corresponding, radical modification of the critical properties at the QCP (at $n_c = 0.805$) is found also nu-

merically in DGA, see Fig. 2 (3rd column). Here, the critical exponents change to $\nu = 0.9 (\pm 0.1)$ and $\gamma = 0.6 (\pm 0.1)$ (with an additional error of the same magnitude stemming from the selection of the proper T range, see Fig. 2; a detailed error analysis can be found in Supplemental Material [53] Sec. II). These exponents are in stark contrast to any standard expectation such as the 3d Heisenberg results or HMM theory, but agree with our RPA exponents. Even when considering the significant error bars, it is safe to say that only the Kohn-anomaly scenario is consistent with our DGA results as these irrevocably show a roughly *linear* behavior of $\xi^{-1}(T)$ in the whole low- and intermediate T -regime above the QCP (i.e., $\nu \approx 1$) and, even more clear-cut, a *strong violation* of the scaling relation $\gamma = 2\nu$ [62], implying a highly non-trivial anomalous dimension η .

Slightly overdoping the system (4th column of Fig. 2, $n=0.79$) yields a Fermi-liquid with a finite χ for $T \rightarrow 0$. In the quantum critical regime (i.e., excluding the low-temperature points which lie outside the quantum critical region) we find similar exponents as at optimal doping ($\nu \approx 1.0, \gamma \approx 0.9$; the determination of the accurate value of the critical exponent γ is more difficult because of the restricted temperature range).

No univocal prediction can be made instead for the *dynamical* exponent z : The frequency dependence of $\chi_{\mathbf{q}}(\omega)$ in the presence of Kohn anomalies has a rather complicated form [22, 61], *not* characterized by a single exponent. The same effect is also responsible for a non-Fermi-liquid power-law in the 2d self energy [22].

Having whole *lines* of Kohn points and hence the above critical exponents is evidently specific to the 3d dispersion with nearest neighbor hopping. Consistent with the results of previous studies [19], however, we demonstrate in Sec. I D of the Supplemental Material [53] that the critical exponents are $\nu = \gamma = 1$ for the more general situations of a FS with *isolated* Kohn points having opposite masses in two directions. This again violates the HMM prediction. Please note that these values of the exponents in 3d coincide (up to logarithmic corrections) [60] with those expected for Kohn points in 2d [21].

In general, the momentum dependence of vertex corrections beyond RPA and the self-energy corrections should not be too strong, and the quasiparticle damping should be sufficiently small at $T \rightarrow 0$ to preserve the above-mentioned values of the critical exponents in the interacting model. Under these assumptions, we expect the observed behavior to be universal, with several new 'universality classes' depending on whether there are lines of Kohn points with divergent or non-divergent mass, or isolated Kohn points with opposite masses (see Supplemental Material [53]).

The final outcome of our calculations, i.e. unusual values of ν, γ and of their mutual relation which are in a different universality class than HMM theory, can be understood thus as the consequence of two competing

physical processes at work: On the one hand, as $T_N \rightarrow 0$ at the QCP, the temporal fluctuations increase the effective dimension of the system above the three geometrical ones. This pushes it above the upper critical dimension and renders non-Gaussian fluctuations irrelevant as in HMM. On the other hand, the effect of Kohn anomalies, yielding a non-analytic momentum- and temperature dependence of the susceptibility, are no longer smeared out by finite T and become relevant.

Conclusions. We have studied the magnetic QCP in the doped $3d$ Hubbard model. We find that, even above the upper critical dimension, quantum criticality is *not* of standard Hertz-Millis-Moriya type. Even in the presence of strong correlations critical properties are driven by Fermi-surface features: the presence of Kohn points leads to unexpected critical exponents, the breakdown of the scaling relations and not univocal definitions of the dynamical exponent z . The implications of our results go well beyond the specific system considered and also hold for other dispersion relations, showing how strongly the QCP physics can be driven by peculiar features of the FS. In this perspective, the cases where controversial interpretations of experiments in the proximity of QCPs arise might need to be reconsidered.

Acknowledgments. We thank G. Rohringer, A. Eberlein, W. Metzner and S. Paschen for insightful discussions and dedicate our work in memory of Walter Kohn and his multitudinous, groundbreaking contributions to solid state physics. We acknowledge support from the Austrian Science Fund (FWF) through the Doctoral School “Building Solids for Function” (TS, FWF project W1243), the project I-610 (TS, AT) and project I 1395-N26 as part of the DFG research unit FOR 1346 (KH), as well as from the European Research Council under the European Union’s Seventh Framework Program (FP/2007-2013)/ERC grant agreement n. 306447 (KH). The work of AK is performed within the theme “Electron” 01201463326 of FASO, Russian Federation and Russian Foundation for Basic Research grant No 17-02-00942. Calculations were performed on the Vienna Scientific Cluster (VSC); we thank J. Zabludil and M. Stöhr for the great support.

[1] H. v. Löhneysen, A. Rosch, M. Vojta, and P. Wölfle, *Rev. Mod. Phys.* **79**, 1015 (2007).
 [2] S. Sachdev, “Quantum Phase Transitions”, Cambridge University Press, Cambridge (1999).
 [3] A. Kopp and S. Chakravarty, *Nature Physics*, **1**, 53 (2005).
 [4] S. Sachdev and B. Keimer, *Quantum Criticality*, *Phys. Today* **64**, 29 (2011).
 [5] T. Moriya and A. Kawabata, *Journ. Phys. Soc. Jpn* **34**, 639 (1973); **35** 669 (1973); T. Moriya “Spin fluctuations in itinerant magnetism”, Springer-Verlag, Berlin, Heidel-

berg, 1985.
 [6] I. E. Dzyaloshinskii and P. S. Kondratenko, *Sov. Phys. JETP* **43**, 1036 (1976).
 [7] J. A. Hertz, *Phys. Rev. B* **14**, 1165 (1976).
 [8] A. J. Millis, *Phys. Rev. B* **48**, 7183 (1993).
 [9] R. Jaramillo, Y. Feng, J. Wang, and T. F. Rosenbaum, *PNAS* **107**, 13631 (2010).
 [10] R. Jaramillo, Y. Feng, J. C. Lang, Z. Islam, G. Srajer, H. M. Ronnow, P. B. Littlewood, and T. F. Rosenbaum, *Phys. Rev. B* **77**, 184418 (2008).
 [11] A. Yeh, Yeong-Ah Soh, J. Brooke, G. Aeppli, T. F. Rosenbaum, and S. M. Hayden, *Nature*, **419**, 459 (2002); M. Lee, A. Husmann, T. F. Rosenbaum, and G. Aeppli, *Phys. Rev. Lett.* **92**, 187201 (2004).
 [12] D. A. Sokolov, M. C. Aronson, L. Wu, Y. Zhu, C. Nelson, J. F. Mansfield, K. Sun, R. Erwin, J. W. Lynn, M. Lumsden, and S. E. Nagler, *Phys. Rev. B* **90**, 035139 (2014).
 [13] A. Schröder, G. Aeppli, R. Coldea, M. Adams, O. Stockert, H. v. Löhneysen, E. Bucher, R. Ramazashvili, and P. Coleman, *Nature* **407**, 351-355 (2000).
 [14] J. Custers, P. Gegenwart, H. Wilhelm, K. Neumaier, Y. Tokiwa, O. Trovarelli, C. Geibel, F. Steglich, C. P’epin, and P. Coleman, *Nature* **424**, 524-527 (2003).
 [15] S. Paschen, T. Lühmann, S. Wirth, P. Gegenwart, O. Trovarelli, C. Geibel, F. Steglich, P. Coleman, and Q. Si, *Nature* **432**, 881 (2004).
 [16] Q. Si, S. Rabello, K. Ingersent, and J. Llewellyn Smith, *Nature* **413**, 804 (2001).
 [17] P. Coleman and A. J. Schofield, *Nature* **433**, 226 (2005).
 [18] W. Kohn, *Phys. Rev. Lett.* **2**, 393 (1959).
 [19] T. M. Rice, *Phys. Rev. B* **2**, 9 (1970).
 [20] F. Stern, *Phys. Rev. Lett.* **18**, 546 (1967).
 [21] T. Holder and W. Metzner, *Phys. Rev. B* **85**, 165130 (2012).
 [22] T. Holder and W. Metzner, *Phys. Rev. B* **90**, 161106 (2014).
 [23] S. Blundell, *Magnetism in Condensed Matter*, Oxford Master Series in Condensed Matter Physics, Oxford University Press (2012).
 [24] J. Hubbard, *Proc. Roy. Soc. London A* **276**, 238 (1963); M. C. Gutzwiller, *Phys. Rev. Lett.* **10**, 159 (1963); J. Kanamori, *Progr. Theor. Phys.* **30**, 275 (1963).
 [25] A. Toschi, A. A. Katanin, and K. Held, *Phys. Rev. B* **75**, 045118 (2007); K. Held, A. A. Katanin, and A. Toschi, *Prog. Theor. Phys. Suppl.* **176**, 117 (2008).
 [26] A. A. Katanin, A. Toschi, and K. Held, *Phys. Rev. B*, **80** 075104 (2009).
 [27] A. Toschi, G. Rohringer, A.A. Katanin, and K. Held, *Annalen der Physik*, **523**, 698 (2011); A. Galler, P. Thunström, P. Gunacker, J. M. Tomczak, and K. Held, *arXiv:1610.02998* (2016).
 [28] G. Rohringer, *New routes towards a theoretical treatment of nonlocal electronic correlations*, PhD thesis, Vienna (2014).
 [29] K. Held, “Dynamical vertex approximation”, edited by E. Pavarini, E. Koch, D. Vollhardt, and A. Lichtenstein, Autumn School on Correlated Electrons. DMFT at 25: Infinite Dimensions, Vol. 4 (Forschungszentrum Jülich, 2014) [arXiv:1411.5191].
 [30] H. Kusunose, *J. Phys. Soc. of Japn.* **79**, 094707 (2010).
 [31] A. N. Rubtsov, M. I. Katsnelson, and A. I. Lichtenstein, *Phys. Rev. B* **77**, 033101 (2008); H. Hafermann, G. Li, A. N. Rubtsov, M. I. Katsnelson, A. I. Lichtenstein, and

- H. Monien, Phys. Rev. Lett. **102**, 206401 (2009).
- [32] C. Slezak, M. Jarrell, Th. Maier, and J. Deisz, J. Phys.: Condens. Matter **21** 435604 (2009).
- [33] A.N. Rubtsov, M. Katsnelson, and A. Lichtenstein, Annals of Physics **327**, 1320 (2012).
- [34] G. Rohringer, A. Toschi, H. Hafermann, K. Held, V. I. Anisimov, and A. A. Katanin, Phys. Rev. B **88**, 115112 (2013).
- [35] C. Taranto, S. Andergassen, J. Bauer, K. Held, A. Katanin, W. Metzner, G. Rohringer, and A. Toschi, Phys. Rev. Lett. **112**, 196402 (2014); N. Wentzell, C. Taranto, A. Katanin, A. Toschi, and S. Andergassen Physical Review B **91**, 045120 (2015).
- [36] G. Li, Phys. Rev. B **91**, 165134 (2015).
- [37] M. Kitatani, N. Tsuji, and H. Aoki, Phys. Rev. B **92**, 085104 (2015).
- [38] T. Ayrál and O. Parcollet, Phys. Rev. B **92**, 115109 (2015).
- [39] T. Ayrál and O. Parcollet, Phys. Rev. B **94**, 075159 (2016).
- [40] A. Georges, G. Kotliar, W. Krauth, and M. Rozenberg, Rev. Mod. Phys. **68**, 13 (1996).
- [41] W. Metzner and D. Vollhardt, Phys. Rev. Lett. **62**, 324 (1989).
- [42] G. Rohringer, A. Valli, and A. Toschi, Phys. Rev. B, **86** 125114 (2012).
- [43] T. Schäfer, G. Rohringer, O. Gunnarsson, S. Ciuchi, G. Sangiovanni, and A. Toschi, Phys. Rev. Lett. **110**, 246405 (2013).
- [44] G. Rohringer, A. Toschi, A. Katanin, and K. Held, Phys. Rev. Lett. **107**, 256402 (2011); T. Schäfer, A. Toschi, and J. M. Tomczak, Phys. Rev. B **91**, 121107(R) (2015).
- [45] A. E. Antipov, E. Gull, and S. Kirchner, Phys. Rev. Lett. **112**, 226401 (2014).
- [46] D. Hirschmeier, H. Hafermann, E. Gull, A. I. Lichtenstein, and A. E. Antipov, Phys. Rev. B **92**, 144409 (2015).
- [47] T. Schäfer, F. Geles, D. Rost, G. Rohringer, E. Arrigoni, K. Held, N. Blümer, M. Aichhorn, and A. Toschi, Phys. Rev. B **91**, 125109 (2015).
- [48] A. L. Rakhmanov, A. V. Rozhkov, A. O. Sboychakov, and Franco Nori, Phys. Rev. B **87**, 075128 (2013).
- [49] T. Wu, H. Mayaffre, S. Krämer, M. Horvatić, C. Berthier, W. N. Hardy, R. Liang, D. A. Bonn, and M.-H. Julien, Nature **477**, 191-194 (2011).
- [50] J. Zaanen and O. Gunnarsson, Phys. Rev. B **40**, 7391(R) (1989); K. Machida, Physica C **158**, 192 (1989); M. Kato, K. Machida, H. Nakanishi and M. Fujita, J. Phys. Soc. Jpn. **59**, 1047 (1990).
- [51] G. Górski, and J. Mozia, Physica B **409**, 71-77 (2013) B **87**, 075128 (2013).
- [52] G. Rohringer and A. Toschi, Phys. Rev. B **94**, 125144 (2016).
- [53] See Supplemental Material accessible at ... for the detailed calculation of the T - and momentum-dependence of $\chi_{\mathbf{q}}$ in the presence of Kohn anomalies, which includes Refs. [54–56].
- [54] L. M. Roth, H. J. Zeiger, and T. A. Kaplan, Phys. Rev. **149**, 519 (1966).
- [55] K. Levenberg, Quart. Appl. Math. **2**, 164-168, (1944), D. Marquardt, SIAM J. Appl. Math. **11**, 431-441, (1963).
- [56] T. Schäfer, *Classical and quantum phase transitions in strongly correlated electron systems*, PhD thesis, TU Wien (2016).
- [57] A. Valli, T. Schäfer, P. Thunström, G. Rohringer, S. Andergassen, G. Sangiovanni, K. Held, and A. Toschi, Phys. Rev. B **91**, 115115 (2015).
- [58] G. Li, N. Wentzell, P. Pudleiner, P. Thunström, and K. Held, Phys. Rev. B **93**, 165103 (2016).
- [59] J. K. Freericks, and M. Jarrell, Phys. Rev. Lett. **74**, 186 (1995), A. N. Tahvildar-Zadeh, J. K. Freericks, and M. Jarrell, Phys. Rev. B **55**, 942 (1997).
- [60] Quantitatively, in $2d$, $\gamma = 1$ with log-corrections[21], differently from the $3d$ unfrustrated result ($\gamma = 0.5$ with much weaker $\ln \ln(1/T)$ corrections). The associated second-order transition can be more difficult to realize in $2d$ [61].
- [61] B. L. Altshuler, L. B. Ioffe, and A. J. Millis, Phys. Rev. B **52**, 5563 (1995).
- [62] Significant violations of $\gamma = 2\nu$, but for a $2d$ system at $T = 0$, have been recently reported by Maier and Strack[63].
- [63] S.A. Maier, and P. Strack, Phys. Rev. B **93**, 165114 (2016).

Supplemental material to "Quantum criticality with a twist - interplay of correlations and Kohn anomalies in three dimensions"

T. Schäfer^a, A. A. Katanin^b, K. Held^a, and A. Toschi^a

^a*Institute of Solid State Physics, TU Wien, 1040 Vienna, Austria and*

^b*Institute of Metal Physics, 620990, Kovalevskaya str. 18, Ekaterinburg, Russia
Ural Federal University, 620002, Mira str. 19, Ekaterinburg, Russia*

I. ANALYTICAL SUSCEPTIBILITY CALCULATIONS IN THE PRESENCE OF KOHN POINTS

To discuss the effect of Kohn anomalies in the 3d Hubbard model, we consider the non-uniform bare susceptibility

$$\chi_{\mathbf{q}+\mathbf{Q}}^0 = - \sum_{\mathbf{k}} \frac{f_{\mathbf{k}} - f_{\mathbf{k}+\mathbf{q}+\mathbf{Q}}}{E_{\mathbf{k}} - E_{\mathbf{k}+\mathbf{q}+\mathbf{Q}}}, \quad (1)$$

where $E_{\mathbf{k}} = -2t(\cos k_x + \cos k_y + \cos k_z) - \mu$ is the electronic dispersion, $\mathbf{Q} \equiv \mathbf{Q}_{T=0} \equiv \mathbf{Q}_0$ is the wave vector of the ground state order, and $f_{\mathbf{k}} \equiv f(E_{\mathbf{k}})$ is the Fermi function. Following the original proposal by W. Kohn[1] and later treatment of Refs. [2, 3], to find anomalous behavior of the susceptibility, we expand the dispersion near the Kohn points \mathbf{K} and $\mathbf{K} + \mathbf{Q}$ at the Fermi surface, which have antiparallel Fermi velocities. To this end we consider, in 3d [2, 3], the saddle point momentum dependence of the dispersion at \mathbf{K} and $\mathbf{K} + \mathbf{Q}$ in the directions transverse to the Fermi velocity \mathbf{v}_F . In case of Kohn lines the dispersion is independent on one of those directions. We find that the susceptibility is maximal at the Kohn points which is, in our experience, a situation not as rare as supposed previously in Ref. [4].

For a simple cubic lattice the susceptibility reaches its maximum at the wavevectors $\mathbf{Q} = (\pi, \pi, Q_z)$. The corresponding Kohn points are easily found to exist for $|\mu| < 2t$ and represent Kohn lines in momentum space (see Fig. 3 e) and f) in the main text) with $K_x \pm K_y = \pm\pi$ and $K_z = -Q_z/2 = -\arccos(-\mu/(2t))$. We parametrize the position of the points on the line by introducing the coordinate $y = \sqrt{2}(\pi/2 \pm K_x)$, such that $|y| < \pi/\sqrt{2}$, $\mathbf{K}_i(y) = (\pm\pi/2 + y/\sqrt{2}, \pm\pi/2 - y/\sqrt{2}, -Q_z/2)$, and $\mathbf{K}_i(y) + \mathbf{Q} = (\mp\pi/2 + y/\sqrt{2}, \mp\pi/2 - y/\sqrt{2}, Q_z/2)$, where $i = 1\dots 4$ enumerates the four Kohn lines, given by the \pm signs.

Expanding the dispersion near the corresponding lines by representing $\mathbf{k} = \mathbf{K}_i(y) + \mathbf{k}_1$ (choosing \mathbf{k}_1 orthogonal to the line), and introducing the rotated coordinate frame ("local" in momentum space) for $\mathbf{k}_1 = (k'_x, k'_y, k'_z)$, by aligning the axis k'_z along the Fermi velocity vector $\mathbf{v}_i(y) = (\nabla E_{\mathbf{k}})_{\mathbf{k}=\mathbf{K}_i(y)+\mathbf{Q}}$, and afterwards rotating the axes $k'_{x,y}$ around the new k'_z axis, such that the axis k'_y is aligned along the Kohn line, we obtain

$$E_{\mathbf{K}_i(y)+\mathbf{k}_1} \simeq -v(y)k'_z + \frac{(k'_x)^2}{2m_x(y)}, \quad (2a)$$

$$E_{\mathbf{K}_i(y)+\mathbf{Q}+\mathbf{k}_1} \simeq v(y)k'_z + \frac{(k'_x)^2}{2m_x(y)}, \quad (2b)$$

where $v(y) \equiv |\mathbf{v}_{\mathbf{K}_i(y)}| = 2t\sqrt{1 + 2\cos^2(y/\sqrt{2}) - \mu^2/(2t)^2}$ and $m_x(y) = -v(y)^2/(8\mu t^2 \cos^2(y/\sqrt{2}))$ are the absolute value of the Fermi velocity and mass at the point $\mathbf{K}_i(y)$ of the line, which do not depend on i . This type of dispersion corresponds to the Kohn singularity of cylindrical symmetry, according to the terminology of Ref. [3], but in our case the dispersion depends on y as a parameter. For fixed y it is identical to that in two dimensions[5-7]; it is also important that in our case the mass diverges at the 2d van Hove points $y = \pm\pi/\sqrt{2}$.

The contribution from the vicinity of Kohn lines to the susceptibility (1) can, thus, be rewritten as

$$\chi_{\mathbf{q}+\mathbf{Q}}^0 = - \sum_i \int_{-\pi/\sqrt{2}}^{\pi/\sqrt{2}} dy \int_{-\Lambda}^{\Lambda} \frac{dk'_x dk'_z}{(2\pi)^3} \frac{f_{\mathbf{K}_i(y)+\mathbf{k}_1} - f_{\mathbf{K}_i(y)+\mathbf{k}_1+\mathbf{q}+\mathbf{Q}}}{E_{\mathbf{K}_i(y)+\mathbf{k}_1} - E_{\mathbf{K}_i(y)+\mathbf{k}_1+\mathbf{q}+\mathbf{Q}}}, \quad (3)$$

where Λ is a cutoff parameter.

A. Influence of Kohn lines at zero temperature

At $T = 0$ for $\mathbf{q} = (q_x, q_x, q_z)$ we obtain from Eq. (3)

$$\chi_{\mathbf{q}+\mathbf{Q}}^0 = \frac{\Lambda}{4\pi^3} \sum_i \int_{-\pi/\sqrt{2}}^{\pi/\sqrt{2}} \frac{dy}{v(y)} \left\{ 2 + \ln \frac{2\Lambda m_x(y)v(y)}{|\Lambda^2 + m_x(y)v(y)\tilde{q}_i(y)|} - 2g_{1/2} \left(\frac{m_x(y)v(y)\tilde{q}_i(y)}{\Lambda^2} \right) \right\}, \quad (4)$$

where

$$g_{1/2}(x) = \sqrt{|x|} \left\{ \begin{array}{ll} \operatorname{artanh}(1/\sqrt{|x|}), & x < -1 \\ \operatorname{arcoth}(1/\sqrt{|x|}), & -1 < x < 0 \\ \arctan(1/\sqrt{x}), & x > 0 \end{array} \right\}, \quad (5)$$

$\tilde{q}_i(y) = q_{ni}(y) + q_{\tau i}(y)^2/(4m_x(y)v(y))$; $q_{ni}(y)$ and $q_{\tau i}(y)$ depend on y and the considered line i . For example, for the line $K_x + K_y = -\pi$ we have

$$\begin{aligned} q_n(y) &= \frac{2t}{v(y)} \left[2q_x \cos(y/\sqrt{2}) + q_z \sqrt{1 - \mu^2/(2t)^2} \right], \\ q_\tau(y) &= \frac{2\sqrt{2}t}{v(y)} \left[q_x \sqrt{1 - \mu^2/(2t)^2} - q_z \cos(y/\sqrt{2}) \right]. \end{aligned} \quad (6)$$

For finite $m_x(y)$ one can expand Eq. (4) at $m_x(y) \max(v(y)\tilde{q}_i(y), T) \ll \Lambda^2$ to reproduce the previously known two-dimensional (cylindrical symmetry) results, integrated over y (cf. Refs. [3, 5, 7])

$$\chi_{\mathbf{q}+\mathbf{Q}}^0 = \frac{1}{4\pi^3} \sum_i \int_{-\pi/\sqrt{2}}^{\pi/\sqrt{2}} \frac{dy}{v(y)} \left[\Lambda \left(2 - \ln \frac{\Lambda}{2m_x(y)v(y)} \right) + \frac{m_x(y)v(y)\tilde{q}_i(y)}{\Lambda} - \pi(m_x(y)v(y)\tilde{q}_i(y))^{1/2} \theta(\tilde{q}_i(y)) \right]. \quad (7)$$

However, in our case the mass $m_x(y)$ diverges at the endpoints $y_0 = \pm\pi/\sqrt{2}$ of the Kohn lines as $m_x(y) \simeq a/(y \pm \pi/\sqrt{2})^2$, where $a = (1 - \mu^2/(2t)^2)/(-\mu)$. The calculation of the integrals in Eq. (4) near this divergence and the expansion of the result with $|a| \max(v(y_0)\tilde{q}(y_0), T) \ll \Lambda^2$ yields

$$\chi_{\mathbf{q}+\mathbf{Q}}^0 = (\chi_{\mathbf{q}+\mathbf{Q}}^0)_{\text{nu}} - \frac{1}{2\pi^2} \left(\frac{a|q_z|}{v} \right)^{1/2} \left\{ \pi\theta(-q_z) + \left[2 + \ln \left(\frac{\Lambda^2}{avq_z} \right) \right] \theta(q_z) \right\} \quad (T = 0), \quad (8)$$

where $(\chi_{\mathbf{q}+\mathbf{Q}}^0)_{\text{nu}}$ is the non-universal contribution from the regions of integration over y far from the singular van Hove points, $v = v(y_0) = 2t\sqrt{1 - \mu^2/(2t)^2}$, and we have accounted that $\tilde{q}(y_0) = q_z$. The universal contributions in Eq. (8) are expected to yield the dominant part of the momentum dependence at small q_z ; they behave as $|q_z|^{1/2}$, with additional logarithmic corrections at $q_z > 0$, and do not depend on the selected line. The result (8) can also be obtained by considering the contribution of the vicinity of the 2d van Hove points $K = (\pi, 0, -Q_z/2)$ and $(0, \pi, -Q_z/2)$ and expanding the dispersion near these points as $E_{\mathbf{K}+\mathbf{k}} = \pm tk_+k_- - vk_z + v^2k_z^2/(8at^2)$ and $E_{\mathbf{K}+\mathbf{Q}+\mathbf{k}} = \mp tk_+k_- + vk_z + v^2k_z^2/(8at^2)$, where $k_\pm = k_x \pm k_y$.

B. Influence of Kohn lines at finite temperatures

To obtain the susceptibility at finite T , we use the identity [6]

$$f(\varepsilon) = - \int_{-\infty}^{\infty} d\varepsilon' f'(\varepsilon') \theta(\varepsilon' - \varepsilon) = - \int_{-\infty}^{\infty} d\varepsilon' f'(\varepsilon') f_{T=0}(\varepsilon - \varepsilon') \quad (9)$$

where $f'(\varepsilon)$ is the derivative of the Fermi function. Analyzing Eq. (3), we find that a shift of the arguments of the Fermi functions by ε' is equivalent to the shift of $v(y)\tilde{q}(y)$ in Eq. (4) by $2\varepsilon'$ for every y . Introducing the variable

$\varepsilon_0 = 2\varepsilon'$, we obtain

$$\begin{aligned} \chi_{\mathbf{q}+\mathbf{Q}}^0 &= -\frac{\Lambda}{4\pi^3} \sum_i \int_{-\infty}^{\infty} d\varepsilon_0 f' \left(\frac{\varepsilon_0}{2} \right) \\ &\times \int_{-\pi/\sqrt{2}}^{\pi/\sqrt{2}} \frac{dy}{v(y)} \left\{ 2 + \ln \frac{2\Lambda m_x(y)v(y)}{|\Lambda^2 + m_x(y)(v(y)\tilde{q}_i(y) - \varepsilon_0)|} - 2g_{1/2} \left(\frac{m_x(y)(v(y)\tilde{q}_i(y) - \varepsilon_0)}{\Lambda^2} \right) \right\} \end{aligned} \quad (10)$$

Calculating again the integral over y near the divergence and changing the integration variable ε_0 to $q_0 = \varepsilon_0/v$, we find

$$\begin{aligned} \chi_{\mathbf{q}+\mathbf{Q}}^0 &= (\chi_{\mathbf{q}+\mathbf{Q}}^0)_{\text{nu}} + \frac{(av)^{1/2}}{4\pi^2} \int_{-\infty}^{\infty} dq_0 f' \left(\frac{vq_0}{2} \right) |q_0 - q_z|^{1/2} \\ &\times \left\{ \pi\theta(q_0 - q_z) + \left[2 + \ln \frac{\Lambda^2}{av(q_z - q_0)} \right] \theta(q_z - q_0) \right\} \quad (T > 0). \end{aligned} \quad (11)$$

C. Analysis of momentum and temperature dependence

In order to analyze the result given by Eq. (11), in a first step, we substitute the approximation for the Fermi function, suggested in Ref. [3],

$$f(\varepsilon) = \begin{cases} 1, & \varepsilon < -CT, \\ (1 - \varepsilon/(CT))/2, & -CT < \varepsilon < CT, \\ 0, & \varepsilon > CT \end{cases} \quad (12)$$

(C is some constant) with $f'(\varepsilon) = -\theta(CT - |\varepsilon|)/(2CT)$ to obtain

$$\chi_{\mathbf{q}+\mathbf{Q}}^0 = (\chi_{\mathbf{q}+\mathbf{Q}}^0)_{\text{nu}} - \frac{\sqrt{a}}{12\pi^2 CT v} \left[(2CT + q_z v)^{3/2} \ln \frac{\Lambda^2}{a(2CT + q_z v)} + \pi(2CT - q_z v)^{3/2} \right] \quad (13)$$

Neglecting the momentum dependence of $(\chi_{\mathbf{q}+\mathbf{Q}}^0)_{\text{nu}}$, we find from Eq. (13) the shift $\delta\mathbf{Q}_T$ of the peak position of the susceptibility with temperature

$$\delta Q_z \simeq -2CT/v \quad \text{with} \quad \delta\mathbf{Q}_T = \mathbf{Q}_T - \mathbf{Q}_0 = (0, 0, \delta Q_z) \quad (14)$$

and the form of its expansion near this temperature-dependent maximum $\delta\mathbf{Q}_T$

$$\chi_{\mathbf{Q}+\mathbf{q}}^0 \simeq (\chi_{\mathbf{Q}}^0)_{T=0} - AT^{1/2} - B \frac{(q_z - \delta Q_z)^2}{T^{3/2}} \quad (15)$$

with some positive constants A, B, C . In the random-phase approximation $\chi_{\mathbf{Q}+\mathbf{q}} = (1/\chi_{\mathbf{Q}+\mathbf{q}}^0 - U)^{-1}$ this implies Eq. (2) of the main text and, hence, the corresponding non-HMM values of the (quantum) critical exponents $\gamma = 1/2$ and $\nu = 1$ for the T -dependence of the magnetic susceptibility and coherence length, respectively. For the latter, we are referring here to the length-scale *parallel* to the z -axis and it is determined by the relative T -dependence of the A and B terms which is $\sim \xi^{-2}$. Much weaker momentum dependences of the magnetic susceptibility, and hence correspondingly smaller correlation lengths, are obviously found in the tangential directions.

To study the properties of the bare susceptibility beyond the approximation Eq. (12), we substitute the derivative of the Fermi function $f'(\varepsilon) = -1/(4T \cosh^2(\varepsilon/(2T)))$ to the Eq. (11). Without logarithmic terms on the right-hand side of Eq. (11), we would obtain again Eqs. (13) and (15). To study corrections to this behavior, let us consider the limit of very low temperatures, and expand Eq. (11) at negative q_z with $|q_z| \gg T/v$ (the limit, which we justify a posteriori, similarly to Ref. [6]). In this case we find:

$$\chi_{\mathbf{q}+\mathbf{Q}}^0 = (\chi_{\mathbf{q}+\mathbf{Q}}^0)_{\text{nu}} - \frac{(aT)^{1/2}}{2\pi v} \left[\left(\frac{v|q_z|}{T} \right)^{1/2} + \frac{1}{(2\pi)^{1/2}} e^{q_z v/(2T)} \ln \frac{2\Lambda^2 e^\gamma}{aT} \right] \quad (T > 0, q_z < 0, v|q_z| \gg T). \quad (16)$$

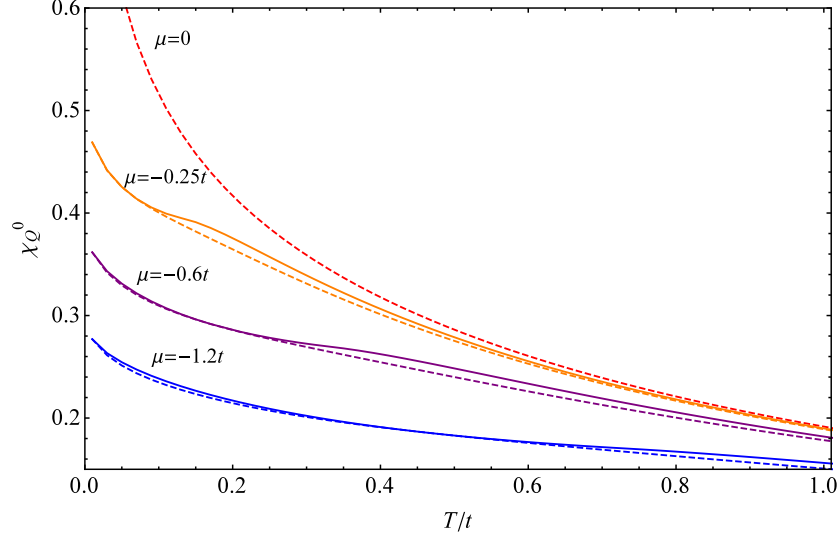


FIG. 1: (color online). Temperature dependences of bare susceptibilities $\chi_{\mathbf{q}}^0$ at the wavevector $\mathbf{q} = \mathbf{Q}_0$, fixed at the maximum of the susceptibility at $T = 0$ (dashed lines) and $\mathbf{q} = \mathbf{Q}_T$, fixed at the temperature-dependent maximum of the susceptibility (solid lines) for different chemical potentials μ .

where γ is the Euler constant. For the position of the maximum of the susceptibility we find the equation

$$\frac{v|\delta Q_z|}{T} = 2 \ln \left[\frac{1}{(2\pi)^{1/2}} \ln \frac{2\Lambda^2 e^\gamma}{aT} \right] + \ln \left(\frac{v|\delta Q_z|}{T} \right) \quad (17)$$

Solving this by iteration, we obtain

$$\frac{v|\delta Q_z|}{T} = 2 \ln \left[\frac{1}{(2\pi)^{1/2}} \ln \frac{2\Lambda^2 e^\gamma}{aT} \right] + \ln \left\{ 2 \ln \left[\frac{1}{(2\pi)^{1/2}} \ln \frac{2\Lambda^2 e^\gamma}{aT} \right] \right\} + \dots, \quad (18)$$

which justifies the assumption $|q_z| \gg T/v$ near the maximum. For the susceptibility at the temperature-dependent maximum $\delta \mathbf{Q}_T = (0, 0, \delta Q_z)$ we then obtain,

$$\chi_{\mathbf{Q}+\delta \mathbf{Q}_T}^0 \simeq (\chi_{\mathbf{Q}+\delta \mathbf{Q}_T}^0)_{\text{nu}} - \frac{1}{2\pi v} \left\{ 2aT \ln \left[\frac{1}{(2\pi)^{1/2}} \ln \frac{2\Lambda^2 e^\gamma}{aT} \right] \right\}^{1/2} \quad (19)$$

while for its second derivative

$$(\partial_{q_z}^2 \chi_{\mathbf{Q}+\mathbf{q}}^0)_{\mathbf{q}=\delta \mathbf{Q}_T} \simeq - \frac{va^{1/2}}{8\pi T^{3/2} \left\{ 2 \ln \left[\frac{1}{(2\pi)^{1/2}} \ln \frac{2\Lambda^2 e^\gamma}{aT} \right] \right\}^{1/2}}. \quad (20)$$

One can see, therefore, that the exact Fermi function yields only weak $\ln(1/T)$ corrections to the factors A, B and C in Eq. (15).

At $\max(v(y)\tilde{q}(y), T) \gg \Lambda^2/|a| \sim \Lambda^2|\mu|$ the temperature dependences (13) and (15) change to the logarithmic behavior, which is characteristic for the commensurate susceptibility at $\mu = 0$. By considering a continuum model we obtain

$$\chi_{\mathbf{q}+\mathbf{Q}}^0 \simeq (\chi_{\mathbf{q}+\mathbf{Q}}^0)_{\text{nu}} = \Lambda \left(1 + \ln \frac{\Lambda}{CT} \right), \quad T \gg \Lambda^2|\mu|. \quad (21)$$

Between the two regimes, we find a narrow region of (almost) linear behavior of the bare susceptibility, reflecting the crossover from the low- to high-temperature behavior (see Fig. 1). In the random phase approximation this implies that the full susceptibility obeys the Curie-Weiss law,

$$\chi_{\mathbf{Q}+\delta \mathbf{Q}_T} \simeq A_P(T - T_P)^{-1} \quad (22)$$

not too close to the Néel temperature T_N . Here, $T_P > T_N$ is the "paramagnetic Néel temperature", in the continuum model $T_P \sim \Lambda^2|\mu|$. The dependence (22) can be further enhanced (and the corresponding temperature region widened) by correlations.

D. Comparison to the effect of the other types of Kohn points

Let us consider the generic pair of Kohn points \mathbf{K} and $\mathbf{K} + \mathbf{Q}$, which belong to the Fermi surface and have opposite Fermi velocities, $\mathbf{v}_{\mathbf{K}} \equiv (\nabla E_{\mathbf{k}})_{\mathbf{k}=\mathbf{K}} = -\mathbf{v}_{\mathbf{K}+\mathbf{Q}}$. Representing $\mathbf{k} = \mathbf{K} + \mathbf{k}_1$, expanding the dispersion near the Kohn points (i.e. at small \mathbf{k}), and introducing again the "local" (in momentum space) rotated coordinate frame $(k'_x, k'_y, k'_z) = R\mathbf{k}_1$ (R is the corresponding rotation matrix), which is obtained by aligning the axis k'_z along the Fermi velocity vector $\mathbf{v}_{\mathbf{K}+\mathbf{Q}} = (\nabla E_{\mathbf{k}})_{\mathbf{k}=\mathbf{K}+\mathbf{Q}}$, and rotating subsequently the axes $k'_{x,y}$ to diagonalize the quadratic form of the dispersion with respect to $k'_{x,y}$ (i.e. excluding the term $k'_x k'_y$), we find

$$E_{\mathbf{K}+\mathbf{k}_1} \simeq -vk'_z + \frac{(k'_x)^2}{2m_x} + \frac{(k'_y)^2}{2m_y}, \quad (23a)$$

$$E_{\mathbf{K}+\mathbf{Q}+\mathbf{k}_1} \simeq vk'_z + \frac{(k'_x)^2}{2m_x} + \frac{(k'_y)^2}{2m_y}, \quad (23b)$$

where $v = |\mathbf{v}_{\mathbf{K}}|$ is the absolute value of the Fermi velocity at the Kohn points and $m_{x,y}$ are the respective masses. According to the discussion in Refs. [2, 3], the dispersions (23) yield the maximum of the susceptibility at the wavevector $\mathbf{q} = \mathbf{Q}$ if and only if $m_x^{-1} = 0$ or $m_y^{-1} = 0$ (we refer to this case as cylindrical Kohn points), or $m_x m_y < 0$ (referred to in the following as hyperbolic Kohn points).

Because of the vanishing of one of the inverse masses, in three dimensions the cylindrical Kohn points form pairs of lines in momentum space, shifted by the wavevector \mathbf{Q} ; at each pair of the points \mathbf{K} and $\mathbf{K} + \mathbf{Q}$ of these lines the dispersions (23) coincide with those for the Kohn points in two dimensions. For a finite mass m_x along the lines (we assume here that $m_y^{-1} = 0$) the momentum dependence of $T = 0$ susceptibility is given by the Eq. (7), where in three dimensions the integral over y is taken along the line of Kohn points. At finite T , straight lines of Kohn points yield the following result, identical to the one previously found in two dimensions [7]:

$$\begin{aligned} \delta Q_z^{2d} &\simeq -\frac{CT}{v} \ln \frac{\Lambda}{T}, \\ \chi_{\mathbf{Q}+\mathbf{q}}^{0,2d} &\simeq (\chi_{\mathbf{Q}}^{0,2d})_{T=0} - AT \ln \frac{\Lambda}{T} - B \frac{(\tilde{q}_z - \delta Q_z^{2d})^2}{T} \end{aligned} \quad (24)$$

with $\tilde{q}_z = q_z + q_x^2/(4m_x v)$ and some positive constants A, B, C . The result (24) implies the critical exponents $\gamma = \nu = 1$ at the quantum phase transition in RPA, which are different from HMM critical exponents.

We stress that the specific case already treated in the Sec. I A-C is realized when m_x diverges at one point of the Kohn-line. This is associated to a further change the values of the exponent γ (to 0.5), and, thus, to a even stronger violation of the HMM prediction. In fact, if $m_x \rightarrow \infty$ the resulting susceptibility will be dominated by the momentum expansion around that point: The momentum dependence of the $T = 0$ susceptibility will be then given by Eq. (8) and Eq. (15) with weak $\ln \ln(1/T)$ corrections at finite T .

However, the vanishing of one of the two inverse masses $m_{x,y}$ at the quantum critical point requires fine-tuning of some additional parameter (if not provided by some additional symmetry), and therefore may not be easily realized in realistic systems. Instead, the isolated hyperbolic Kohn points may easily occur, since their appearance is conditioned by the properties of the Fermi surface only. For the pair of hyperbolic points at $T = 0$ one has for $\mathbf{q} = R^{-1}(0,0,q_z)$ (cf. Refs. [2, 3])

$$\chi_{\mathbf{q}+\mathbf{Q}}^{0,\text{hyp}} = (\chi_{\mathbf{Q}}^{0,\text{hyp}})_{\text{nu}} - \frac{|m_x m_y|^{1/2}}{16\pi} |q_z|, \quad (T = 0). \quad (25)$$

The momentum dependence of the susceptibility on q_z is therefore linear; the dependence on the other components of momentum q is quadratic, and can be neglected here for the generic direction of the momentum, which does not yield a vanishing q_z in the rotated coordinate frame. To obtain the susceptibility at finite T , we can again use Eq. (9) and take into account that the shift of the arguments of the Fermi function by $-\varepsilon'$ is equivalent to the shift of q_z by $2\varepsilon'/v$. Therefore, we obtain

$$\begin{aligned} \chi_{\mathbf{Q}+\mathbf{q}}^{0,\text{hyp}} &= - \int_{-\infty}^{\infty} d\varepsilon' f'(\varepsilon') \left[\chi_{\mathbf{Q}+R^{-1}(0,0,q_z+2\varepsilon'/v)}^{0,\text{hyp}} \right]_{T=0} \\ &= (\chi_{\mathbf{Q}}^{0,\text{hyp}})_{\text{nu}} + \frac{|m_x m_y|^{1/2}}{16\pi v} \int_{-\infty}^{\infty} d\varepsilon' f'(\varepsilon') |vq_z + 2\varepsilon'|, \quad (T > 0). \end{aligned} \quad (26)$$

Representing $\varepsilon' = T\tilde{\varepsilon}$ and introducing the dimensionless derivative of the Fermi function $\varphi(\tilde{\varepsilon}) = Tf'(T\tilde{\varepsilon})$, we obtain

$$\chi_{\mathbf{Q}+\mathbf{q}}^{0,\text{hyp}} = (\chi_{\mathbf{Q}}^{0,\text{hyp}})_{\text{nu}} + \frac{T|m_x m_y|^{1/2}}{16\pi v} \int_{-\infty}^{\infty} d\tilde{\varepsilon} \varphi(\tilde{\varepsilon}) \left| \frac{vq_z}{T} + 2\tilde{\varepsilon} \right| \quad (27)$$

In the approximation (12) we find

$$\begin{aligned} \chi_{\mathbf{Q}+\mathbf{q}}^{0,\text{hyp}} &= (\chi_{\mathbf{Q}}^{0,\text{hyp}})_{\text{nu}} - \frac{T|m_x m_y|^{1/2}}{32C\pi v} \int_{-C}^C d\tilde{\varepsilon} \left| \frac{vq_z}{T} + 2\tilde{\varepsilon} \right| \\ &= (\chi_{\mathbf{Q}}^{0,\text{hyp}})_{\text{nu}} - \frac{|m_x m_y|^{1/2}}{16\pi} \times \begin{cases} |q_z|, & |q_z| > CT/(2v), \\ \frac{CT}{v} + \frac{vq_z^2}{4CT}, & |q_z| < CT/(2v), \end{cases} \end{aligned} \quad (28)$$

in agreement with the result of Ref. [3]. To verify that this result does not change qualitatively by using the exact Fermi function, we substitute $\varphi(\tilde{\varepsilon}) = -1/(4 \cosh^2(\tilde{\varepsilon}/2))$ in Eq. (27) to obtain

$$\begin{aligned} \chi_{\mathbf{Q}+\mathbf{q}}^{0,\text{hyp}} &= (\chi_{\mathbf{Q}}^{0,\text{hyp}})_{\text{nu}} - \frac{T|m_x m_y|^{1/2}}{64\pi v} \int_{-\infty}^{\infty} \frac{d\tilde{\varepsilon}}{\cosh^2(\tilde{\varepsilon}/2)} \left| \frac{vq_z}{T} + 2\tilde{\varepsilon} \right| \\ &= (\chi_{\mathbf{Q}}^{0,\text{hyp}})_{\text{nu}} - \frac{T|m_x m_y|^{1/2}}{4\pi v} \ln \left[2 \cosh \left(\frac{vq_z}{4T} \right) \right], \quad (T > 0). \end{aligned} \quad (29)$$

At large $q_z \gg T/v$ we return to the $T = 0$ result, Eq. (25). Expanding Eq. (29) near the maximum at $q_z = 0$ we find:

$$\chi_{\mathbf{Q}+\mathbf{q}}^{0,\text{hyp}} \simeq (\chi_{\mathbf{Q}}^{0,\text{hyp}})_{\text{nu}} - \frac{T|m_x m_y|^{1/2}}{4\pi v} \left[\ln 2 + \frac{1}{2} \left(\frac{vq_z}{4T} \right)^2 \right], \quad q_z \ll T/v. \quad (30)$$

The result (30) yields the same critical exponents obtained by means of RPA for the quantum phase transition, in 2d ($\gamma = \nu = 1$) without logarithmic corrections. Therefore, in all the cases when Kohn points yield the maximum of the susceptibility, we obtain critical exponents at the quantum critical point, which significantly differ from the critical exponents of the Hertz-Moriya-Millis theory.

II. NUMERICAL DETAILS ON THE DETERMINATION OF THE (QUANTUM) CRITICAL EXPONENTS

As already briefly mentioned in the main text, the numerical determination of the critical exponents γ and ν in the quantum critical region is rather challenging. In order to obtain the fixed-doping temperature cuts shown in Fig. 2 of the main text and, in particular, accurate values (within given error bars) for the critical exponents by means of DGA, the following aspects have to be considered:

- i) *Least square fitting procedure* – First of all, please note, that in each case where fits have to be performed, the method of minimizing the sum of squares (“(non-linear) least square fit” with Levenberg-Marquardt algorithm) has been used [8].
- ii) *Frequency extrapolation* – A careful frequency extrapolation in terms of (internal) Matsubara frequencies must be performed for the quantities of interest (i.e., the non-uniform spin-susceptibility $\chi(\omega, \mathbf{q})$ and the magnetic correlation length ξ) in order to control finite-size effects stemming from a finite amount of Matsubara frequencies in the internal summations (see also discussion in [9]). This is done by calculating χ and ξ with increasing number of frequencies n_ω (limited by computational time) and extrapolating them by fitting with the following function

$$f(n_\omega) = a + \frac{b}{n_\omega}, \quad (31)$$

where a gives the result of the extrapolated quantity for $n_\omega \rightarrow \infty$. Considering also the next order term ($\frac{c}{n_\omega^2}$) of Eq. (31) does not alter the result much. Of course, this extrapolation leads to error bars for both observables, χ and ξ . However, the size of the corresponding errors is so small that they are not visible on the scale of Fig. 2 of

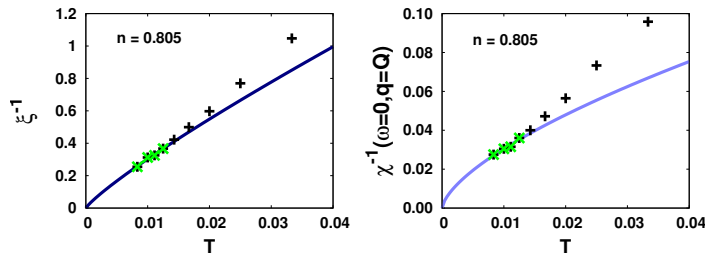


FIG. 2: (color online) Inverse correlation length (ξ^{-1} , left panel) and maximal susceptibility (χ^{-1} , right panel), obtained by DGA, as a function of temperature. The blue lines show the fits for extracting the critical exponents ν and γ using the four lowest temperature points.

the main text. We also note that the extraction of the correlation length ξ is carried out by a fit of a Lorentzian fit function

$$\chi(\omega=0, \mathbf{q}) = \frac{A}{(\mathbf{q} - \mathbf{Q})^2 + \xi^{-2}} \quad (32)$$

simultaneously with the determination of the peak \mathbf{Q} where the static susceptibility $\chi(\omega = 0, \mathbf{q})$ reaches its maximum. This procedure again results in error bars not visible in the plots of Fig. 2 in the main text. Let us stress that the error stemming directly from the exact diagonalization (ED) impurity solver (bath discretization), cannot easily be estimated. In particular, as in previous calculations with ladder-DGA [10, 11], the DMFT vertex functions have been computed with a discretization of five sites (4 bath and 1 impurity site), whereas the corresponding parameters of the auxiliary Anderson impurity model for different DMFT calculation at the same doping have been obtained by an annealing procedure (from high to low temperatures). With this set-up it was possible to get reasonable convergence in the temperature interval shown in the figures (but not below).

- iii) *Momentum grids* – The momentum grid used for internal summations (used, e.g., in the construction of the momentum-resolved DMFT susceptibility) has to be converged [9]. A typical number of points for a converged resolution of the fully irreducible Brillouin zone is 30^3 . In this respect, let us further note that, in general, the numerical values for the correlation length ξ seem to be much more stable than the ones for the susceptibility χ (w.r.t. the number of Matsubara frequencies and the momentum grid). This might be a consequence of the incommensurability of the magnetism, which mostly affects the changes in the position of the maximum of the susceptibility.
- iv) *Fitting region* – In general, the extension of the (quantum) critical region within the phase diagram is not known a priori, so that data points lying outside this region (e.g. at high temperatures) might need to be excluded from the numerical fit of the quantum critical exponents. In our case this is particularly delicate since, among other effects, we have a crossover from commensurate to incommensurate fluctuations with temperature [this can be clearly seen, e.g., for $n = 0.87$ in Fig. 2 of the main text]. In particular, when considering the most important regime at the (estimated) position of the QCP ($n = 0.805$), we obtained the results summarized in Fig. 2 of this Supplemental Material. The figure shows the DGA data as well as the fitted functions for a temperature cut at the quantum critical doping value ($n = 0.805$) for the (inverse) magnetic correlation length (left panel) and the magnetic susceptibility (right panel). The DGA data points are marked in black (solid line), the points which are used for the fit are green (crossed) and the fit-function, from which the critical exponents are extracted, is colored blue (solid line). Note the clear deviation from the critical (asymptotic) behavior for the non-green points in Fig. 2 (right panel). The critical exponents are determined using the following fit-functions:

$$\xi^{-1}(T) = AT^\nu, \quad \chi^{-1}(\omega = 0, \mathbf{q} = \mathbf{Q}; T) = BT^\gamma. \quad (33)$$

The results for both critical exponents unavoidably depend on the number $\#$ of (low) temperature points used for the fit. We have fitted $\# = 2, 3, 4, 5$ points to Eq. (33) and obtained an average (standard deviation) over all these four fits of $\nu = 0.93 (\pm 0.09)$ and $\gamma = 0.61 (\pm 0.06)$, respectively. We have also calculated the error of each particular fit. For $\# = 4$, e.g., the fits yield $A = 18.6, \nu = 0.86$ and $B = 1.3, \gamma = 0.65$, with the covariance matrices shown in Tab. iv for the estimated prefactors and exponents of Eq. (33):

This corresponds to standard deviations (square roots of the respective main diagonal entries of the covariance

	A	ν		B	γ
A	48.8	0.69	B	0.10	0.04
ν	0.69	0.01	γ	0.04	0.01

TABLE I: Covariance matrices of the fits for the critical exponents ν (left) and γ (right) at $n=0.805$ via Eq. (33) for $\# = 4$ temperature points used. Note that the determined coefficients A and B are much larger than ν and γ , respectively.

matrix) of $\sigma_\nu = 0.09$ and $\sigma_\gamma = 0.1$. That is, altogether, we can estimate $\nu = 0.9 (\pm 0.1)$ and $\gamma = 0.6 (\pm 0.1)$, as given in the main text.

Let us note that there are numerical limitations, which prevent the reliable calculation of the DMFT(ED) vertex input for D Γ A at lower temperatures (restrictions of the number of discrete bath sites, Matsubara frequencies as well as momentum grid points). Additionally, as mentioned in (iv), at higher temperatures, there are deviations from the critical behavior, because we are outside the asymptotic quantum critical region. For these reasons, the actual uncertainty of the numerical fit might be somewhat larger. However, our numerical analysis is reaffirmed by obtaining different fits yielding ν and γ values in agreement with our analytical calculations $\nu = 1$ and $\gamma = 0.5$. Furthermore, the exponent $\nu = 1$ is also in agreement with the one obtained at $n = 0.79$ in Fig. 2 of the main text. Here the linear behavior $\xi^{-1} \propto T$ is found in an “intermediate” temperature-regime, consistent with the expectation of the location of the quantum critical region away slightly from the QCP. This result is perfectly compatible with the typical funnel-like shape of the quantum critical regime, which implies that also the lowest temperature points have to be excluded from the fit, because of their location outside the quantum critical regime. This additional limitation makes a precise determination of the critical exponents for $n = 0.79$ more difficult (and, especially, of the most sensible one for the fitting procedure, i.e. γ).

Hence, in conclusion, we can state that our D Γ A results (even with a possibly larger error) strongly violate the conventional scaling relation $\gamma = 2\nu$ in the quantum critical region of the three-dimensional Hubbard model, and are numerically compatible with the analytic RPA prediction of $\gamma=0.5$ and $\nu=1.0$.

-
- [1] W. Kohn, Phys. Rev. Lett. **2**, 393 (1959).
 - [2] L. M. Roth, H. J. Zeiger, and T. A. Kaplan, Phys. Rev. **149**, 519 (1966).
 - [3] T. M. Rice, Phys. Rev. B **2**, 3619 (1970).
 - [4] H. v. Löhneysen, A. Rosch, M. Vojta, and P. Wölfle, Rev. Mod. Phys. **79**, 1015 (2007).
 - [5] F. Stern, Phys. Rev. Lett. **18**, 546 (1967).
 - [6] T. Holder and W. Metzner, Phys. Rev. B **85**, 165130 (2012).
 - [7] T. Holder and W. Metzner, Phys. Rev. B **90**, 161106 (2014).
 - [8] K. Levenberg, Quart. Appl. Math. **2**, 164-168, (1944), D. Marquardt, SIAM J. Appl. Math. **11**, 431-441, (1963).
 - [9] T. Schäfer, *Classical and quantum phase transitions in strongly correlated electron systems*, PhD thesis, TU Wien (2016).
 - [10] G. Rohringer, A. Toschi, A. Katanin, and K. Held, Phys. Rev. Lett. **107**, 256402 (2011); T. Schäfer, A. Toschi, and J. M. Tomczak, Phys. Rev. B **91**, 121107(R) (2015).
 - [11] T. Schäfer, F. Geles, D. Rost, G. Rohringer, E. Arrigoni, K. Held, N. Blümer, M. Aichhorn, and A. Toschi, Phys. Rev. B **91**, 125109 (2015).